Three-Dimensional Calculation of Transonic Viscous Flows by an Implicit Method

H. Hollanders,* A. Lerat,† and R. Peyret‡
Office National d'Etudes et de Recherches Aérospatiales (ONERA), Chatillon, France

A new implicit finite- volume method for solving the three-dimensional Navier-Stokes equations for compressible fluids is presented and applied to the calculation of flows over swept wings at moderate Reynolds numbers. The method makes use of an explicit predictor-corrector scheme to calculate a provisional value, which is then corrected by using an implicit operator. The explicit part is a generalization of the centered Thommen scheme, while the implicit operator is a combination of the inviscid schemes proposed by Lerate and the viscous treatment of Beam and Warming. Results are here presented for a swept wing between two parallel walls and for the finite wing ONERA M6 at $M_\infty = 0.8$, zero incidence and $Re_\infty = 1000$. The computations are performed with a time-step about 5 to 10 times greater than the explicit step.

I. Introduction

In the last decade, several Navier-Stokes codes have been developed in order to calculate two- or three-dimensional viscous compressible flows using explicit, hybrid, or implicit methods. A general review of Navier-Stokes solvers can be found in Refs. 1-4. In order to reduce the computing costs for complex flowfields, most current research makes use of implicit methods.[5-9] All of these methods deal with the governing equations in conservative form and use a time linearization procedure associated with the ADI factorization which leads to the inversion of algebraic linear systems with either a block-tridiagonal[5-7] or a block-bidiagonal[8,9] structure.

In the method developed by Briley and MacDonald,[5] the unknowns of the block-tridiagonal linear systems are the primitive variables (density, velocity, and temperature), whereas in the method of Beam and Warming,[6] they are the conservative variables (density, momentum, and total energy). It should be noted that the choice of the conservative variables is well suited to the prediction of unsteady flows with shocks at high Reynolds numbers. In both methods, the time discretization makes use of first-order approximation (backward Euler) or second-order approximation (Crank-Nicolson, three-point backward), and the space derivatives are replaced by central differences. As a result, the implicit schemes are not dissipative in the sense of Kreiss in the inviscid limit. Moreover, for a scalar model equation (the Burgers equation), it can be shown that the tridiagonal linear systems are not always diagonally dominant. These methods are unconditionally stable in one and two space dimensions, but they become unstable in the inviscid three-dimensional case due to the ADI factorization. For large Reynolds number flows, this loss of stability is a serious drawback. In order to remove these shortcomings, the above authors have added some artificial viscosity terms. In addition, Steger[7] has replaced the centered differences in space by upwind approximations in the supersonic regions.

In the approach of MacCormack,[8,9] the block-bidiagonal structure results from 1) the alternate use of two-point noncentered operators at predictor and corrector steps for the spatial differencing of the inviscid terms, and 2) the use of a modified Saul'ev scheme for the viscous terms. The method is unconditionally stable and it is second-order accurate in the inviscid case. When viscosity is predominant, accuracy is obtained under a certain constraint on the time step with respect to the mesh size. Concerning the linear algebraic structure, it appears that one block-tridiagonal system of the previous methods[5-7] is replaced by two block-bidiagonal systems in the MacCormack method.[8,9] Therefore, the computational costs of the matrix inversions in both approaches seem to be similar.

The purpose of this investigation is to develop a new implicit method for solving the compressible Navier-Stokes equations with applications to three-dimensional flows. The present method is well suited to the calculations at high Reynolds numbers since it extends an algorithm devised for the Euler equations, which is the method proposed by Lerat[10-11] and applied to two-dimensional transonic flows by Lerat, Sides, and Daru.[12] This inviscid method retains the advantages of the Beam and Warming approach for the Euler equations,[13] namely, the conservative form, the second-order accuracy in space, the stability in one and two dimensions, and the use of block-tridiagonal linear systems. However, as the above-mentioned shortcomings are removed, the inviscid method is unconditionally stable, even in three dimensions, and dissipative in the sense of Kreiss, and it leads to the solution of well-conditioned linear systems.

In the new method, the treatment of the viscous and inviscid terms is coupled. However, if the inviscid fluxes should vanish, the implicit method would reduce to the Crank-Nicolson scheme.

The present method includes two computational stages. In the first one, a provisional value is calculated by using an explicit predictor-corrector scheme, which is a generalization of the centered Thommen scheme.[14] In the second stage, where the "delta" formulation is used, the provisional value is corrected by implicit operators factorized with the ADI technique. This implicit stage requires only the solution of block-tridiagonal linear systems.

The implementation of the new method is performed through a finite-volume approach, using three-dimensional curvilinear meshes.

The formulation of the method is presented in Sec. II for a model equation in one dimension. Then, in Sec. III, the extension to the three-dimensional Navier-Stokes equations is

Presented as Paper 83-1953 at the AIAA Sixth Computational Fluid Dynamics Conference, Danvers, MA, July 13-15, 1983; received Nov. 17, 1983; revision received Nov. 28, 1984.

*Head, Research Group.
†Consultant; also, Professor, Ecole Nationale Supérieure des Arts et Métiers, Paris, France.
‡Consultant; also, Research Director, Centre National de la Recherche Scientifique, Université de Nice, France.

described using the finite volume approach. Finally, applications of the method are presented in Sec. IV, corresponding to steady laminar flows in two and three dimensions. The goal of these applications is to test the method in a configuration including reverse flow regions and wakes at moderate Reynolds numbers.

II. One-Dimensional Method

The method is described by considering the simple one-dimensional scalar equation

$$\frac{\partial w}{\partial t}+\frac{\partial}{\partial x}\left[g\left(w,\frac{\partial w}{\partial x}\right)\right]=0 \tag{1a}$$

where

$$g\left(w,\frac{\partial w}{\partial x}\right)=f(w)-\nu(w)\frac{\partial w}{\partial x} \tag{1b}$$

with $\nu(w)\geq 0$. The approximation in time ($t=n\Delta t$) is constructed via the Taylor expansion,

$$w^{n+1}=w^n+\Delta t\left(\frac{\partial w}{\partial t}\right)^n+\frac{\Delta t^2}{2}\left(\frac{\partial^2 w}{\partial t^2}\right)^n+\mathcal{O}(\Delta t^3) \tag{2}$$

in which Eq. (1a) is used, so that

$$w^{n+1}=w^n-\Delta t\left(\frac{\partial g}{\partial x}\right)^n-\frac{\Delta t^2}{2}\frac{\partial}{\partial x}\left(\frac{\partial g}{\partial t}\right)^n+\mathcal{O}(\Delta t^3) \tag{3}$$

The time derivative $\partial g/\partial t$ is evaluated using Eq. (1b),

$$\frac{\partial g}{\partial t}=\frac{\partial f}{\partial t}-\frac{\partial}{\partial t}\left(\nu\frac{\partial w}{\partial x}\right)=A\frac{\partial w}{\partial t}-\frac{\partial}{\partial x}\left(\nu\frac{\partial w}{\partial t}\right) \tag{4}$$

where $A=\mathrm{d}f/\mathrm{d}w$.

One of the features of the method is that the two time derivatives $\partial w/\partial t$ occuring in Eq. (4) are approximated in two different ways. For the second term $\partial(\nu\partial w/\partial t)/\partial x$ the standard approximation

$$\left(\frac{\partial w}{\partial t}\right)^n\simeq\frac{w^{n+1}-w^n}{\Delta t}\equiv\frac{\Delta w^n}{\Delta t} \tag{5}$$

is used. On the other hand, for the first term $A\partial w/\partial t$, we consider the following linear combination:

$$\left(\frac{\partial w}{\partial t}\right)^n\simeq 2a\frac{w^{n+1}-w^n}{\Delta t}+bA^n\frac{\partial w^{n+1}}{\partial x}-(1-2a+b)\frac{\partial f^n}{\partial x}$$
$$+(1-2a)\frac{\partial}{\partial x}\left(\nu\frac{\partial w}{\partial x}\right)^n \tag{6}$$

where a and b are two arbitrary parameters. If $\nu=0$, this approximation for $\partial w/\partial t$ reduces to the one previously introduced in Ref. 10.

Approximation (6) is a combination of four terms. The first term with $a=\frac{1}{2}$ corresponds to the Crank-Nicolson approximation and the last two terms with $a=b=0$ correspond to an explicit approximation of the Lax-Wendroff type. The second term in Eq. (6) can be seen as a linearly implicit version of

$$b\frac{\partial f^n}{\partial x}=bA^n\frac{\partial w^n}{\partial x} \tag{7}$$

This implicit term $bA^n(\partial w/\partial x)^{n+1}$ is essential for ensuring dissipation and well-conditioning of the algebraic systems in the inviscid case. More precisely, in this case, the former properties and unconditional stability are achieved when using centered-space differencing (see Refs. 10 and 11) if

$$a<\tfrac{1}{2},\quad b\leq a-\tfrac{1}{2},\ \text{and}\ b<-a^2/4 \tag{8}$$

Now, taking account of Eq. (7) in Eq. (6), this equation becomes

$$\left(\frac{\partial w}{\partial t}\right)^n\simeq\left[2a\frac{\Delta w}{\Delta t}-(1-2a)\frac{\partial g}{\partial x}+bA\frac{\partial}{\partial x}(\Delta w)\right]^n \tag{9}$$

where $\Delta w^n=w^{n+1}-w^n$. Then, bringing Eqs. (4), (5), and (9) into Eq. (3), we obtain the following second-order time-accurate scheme

$$\Delta w^n+a\Delta t\frac{\partial}{\partial w}(A\Delta w)^n+b\frac{\Delta t^2}{2}\frac{\partial}{\partial w}\left[A^2\frac{\partial}{\partial x}(\Delta w)\right]^n$$
$$-\frac{\Delta t}{2}\frac{\partial^2}{\partial x^2}(\nu\Delta w)^n=-\Delta t\frac{\partial g^n}{\partial x}+(1-2a)\frac{\Delta t^2}{2}\frac{\partial}{\partial x}\left(A\frac{\partial g}{\partial x}\right)^n \tag{10}$$

The parameters a and b are assumed to verify inequalities (8).

If space differencing is performed with centered formulas involving 3 points at time level $n+1$ and 5 points at time level n, the resulting scheme is second-order accurate in space as well.

Concerning the choice of the parameters a and b, the analysis of the scheme applied to the Euler equations has led to the following results[15]:

1) For unsteady problems, the truncation error of the scheme can be minimized for large Δt by taking

$$b=a-\tfrac{1}{2} \tag{11}$$

2) For steady problems, the convergence rate of the scheme to the steady state is optimal when

$$b=2a-1 \tag{12}$$

because the spectral radius of the amplification matrix decreases in this case as Δt increases.

Since the accuracy of the steady solution ($\Delta w^n=0$) does not depend on the parameter b [see the right-hand side of Eq. (10)], the choice of Eq. (12) is convenient for steady flow calculations.

The discretization of the derivative

$$\frac{\partial}{\partial x}\left[A\frac{\partial}{\partial x}\left(\nu\frac{\partial w}{\partial x}\right)\right]\ \text{in}\ \frac{\partial}{\partial x}\left(A\frac{\partial g}{\partial x}\right)$$

of Eq. (10) leads to the usual difficulty near a boundary. This difficulty is increased when the scheme is applied to a system of multidimensional equations, particularly when a finite volume approach is used. This shortcoming is removed by using a predictor-corrector procedure to evaluate the right-hand side of Eq. (10).

In the first step, a provisional incremental value $\Delta\hat{w}_i=\hat{w}_i^{n+1}-w_i^n$ is calculated from the predictor-corrector scheme

$$\tilde{w}_{i+\frac{1}{2}}^{n+\alpha}=\bar{w}_{i+\frac{1}{2}}^n-\alpha\Delta t\delta_x(f-\theta\nu\delta_x\bar{w})_{i+\frac{1}{2}}^n \tag{13a}$$

$$\Delta\hat{w}_i=-\Delta t\delta_x\left[\frac{1-2a}{2\alpha}\tilde{f}^{n+\alpha}+\left(1-\frac{1-2a}{2\alpha}\right)\bar{f}^n-\bar{\nu}^n\delta_x w^n\right]_i \tag{13b}$$

where w_i^n is the approximation at $x=i\Delta x$ and

$$\bar{w}_{i+\frac{1}{2}}=(w_{i+1}+w_i)/2, \qquad \delta_x\varphi_{i+\frac{1}{2}}=(\varphi_{i+1}-\varphi_i)/\Delta x$$

$$\tilde{f}_{i+\frac{1}{2}}^{n+\alpha}=f(\tilde{w}_{i+\frac{1}{2}}^{n+\alpha}), \quad \tilde{f}_{i+\frac{1}{2}}^{n}=f(\tilde{w}_{i+\frac{1}{2}}^{n}), \quad \tilde{\nu}_{i+\frac{1}{2}}^{n}=\nu(\tilde{w}_{i+\frac{1}{2}}^{n})$$

The parameter $\alpha(\alpha\neq 0)$ characterizes the time level at which the predicted value is evaluated. In Eq. (13a), θ takes the value of 1 or 0.

In the second step, the final value is calculated from

$$\Delta w_i^n+a\Delta t\delta_x(\bar{A}\overline{\Delta w})_i^n+b\frac{\Delta t^2}{2}\delta_x[\bar{A}^2\delta_x(\Delta w)]_i^n$$

$$-\frac{\Delta t}{2}\delta_x^2(\nu\Delta w)_i^n=\Delta\hat{w}_i \tag{14}$$

with

$$\bar{A}_{i+\frac{1}{2}}^n=A(\tilde{w}_{i+\frac{1}{2}}^n)$$

The value $\theta=1$ ensures the consistency of the approximation (13) with the right-hand side of Eq. (10). In this case, the global scheme (13), (14) is second-order accurate in time and space as shown by the truncation error

$$\epsilon=(1-2a)(1-\theta)\frac{\Delta t}{2}\frac{\partial}{\partial x}\left[A\frac{\partial}{\partial x}\left(\nu\frac{\partial w}{\partial x}\right)\right]+\mathcal{O}(\Delta t^2,\Delta x^2)$$

In the linear case, the scheme (13), (14) is unconditionally stable for $\theta=0$ and for any value of a and b verifying Eq. (8) (the parameter α does not occur in a linearized analysis). However, in the case $\theta=0$ (a value that suppresses the viscous part in the predictor), the scheme is only first-order accurate in time, but the truncation error can be diminished if $a=\frac{1}{2}-\kappa(\kappa\ll 1)$.

For $\theta=1$, the stability has been analyzed through the numerical study of the amplification factor. Figure 1 shows the region of stability (below the curves) in terms of a after elimination of b, using Eq. (11) or (12).

In the inviscid case, the value $a=0$ leads to a simple unconditionally stable scheme that has been successfully applied to the solution of the two-dimensional Euler equations.[12] In the viscous case, stability is no longer unconditional, but large values of the time step can be used if a is chosen within the range $(0,\frac{1}{2})$.

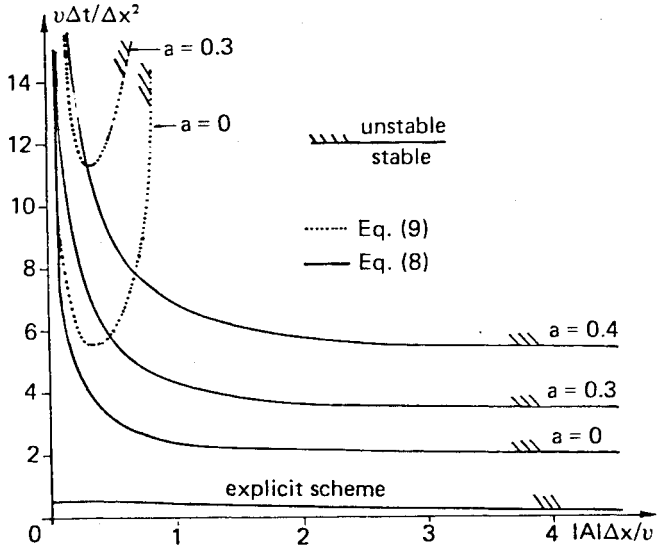

Fig. 1 Region of stability.

III. The Three-Dimensional Method

The scheme described above will now be applied to the solution of the Navier-Stokes equations, using the finite volume approach.

Governing Equations

The integral form of the Navier-Stokes equations for a fixed control volume v is written as

$$\frac{\mathrm{d}}{\mathrm{d}t}\int\int\int_v W\mathrm{d}v+\int\int_S H_\beta N_\beta \mathrm{d}S=0 \tag{15}$$

where S is the boundary of v, N_β $(\beta=1,2,3)$ are the components of the outward normal unit vector $\underline{N}$ to S in a Cartesian frame $(x_\beta,\ \beta=1,2,3)$, and

$$W=(W_\ell)=\begin{bmatrix}\rho\\ \rho u_1\\ \rho u_2\\ \rho u_3\\ \rho E\end{bmatrix} \quad (\ell=1,\ldots,5), \qquad H_\beta=H_\beta^I-H_\beta^v$$

$$H_\beta^I=(H_{\beta\ell}^I)=u_\beta\begin{bmatrix}\rho\\ \rho u_1\\ \rho u_2\\ \rho u_3\\ \rho E\end{bmatrix}+p\begin{bmatrix}0\\ \delta_{\beta 1}\\ \delta_{\beta 2}\\ \delta_{\beta 3}\\ u_\beta\end{bmatrix}$$

$$H_\beta^v=(H_{\beta\ell}^v)=\frac{1}{Re_\infty}\begin{bmatrix}0\\ \tau_{\beta 1}\\ \tau_{\beta 2}\\ \tau_{\beta 3}\\ \tau_{\beta\epsilon}u_\epsilon+\dfrac{\gamma\mu}{Pr}\dfrac{\partial e}{\partial x_\beta}\end{bmatrix}$$

$$\tau_{\beta\epsilon}=\lambda\frac{\partial u_\kappa}{\partial x_\kappa}\delta_{\beta\epsilon}+\mu\left(\frac{\partial u_\beta}{\partial x_\epsilon}+\frac{\partial u_\epsilon}{\partial x_\beta}\right), \quad \begin{pmatrix}\beta=1,2,3\\ \epsilon=1,2,3\end{pmatrix}$$

with the density ρ, velocity $\underline{U}=(u_1,\ u_2,\ u_3)$, specific energy e, total specific energy $E(=e+U^2/2)$, pressure $p=(\gamma-1)\rho e$, the specific heat ratio $\gamma(=1.4)$ and the Kronecker symbol $\delta_{\beta\epsilon}$. The viscosity coefficients λ and μ satisfy $3\lambda+2\mu=0$, and μ varies according to the Sutherland law. The above equations are in dimensionless form, in such a way that $Re_\infty=\rho_\infty U_\infty L/\mu_\infty$ is the Reynolds number based on the freestream conditions and a characteristic length L, and Pr $(=0.72)$ is the Prandtl number.

Time Discretization

First, let us consider the differential form of Eq. (15),

$$\frac{\partial W}{\partial t}+\frac{\partial H_\beta}{\partial x_\beta}=0 \tag{16}$$

By using Eq. (16), the expansion corresponding to Eq. (3) is now

$$\frac{W^{n+1}-W^n}{\Delta t}=\frac{\Delta W^n}{\Delta t}=-\left(\frac{\partial H_\beta}{\partial x_\beta}\right)^n-\frac{\Delta t}{2}\left(\frac{\partial^2 H_\beta}{\partial x_\beta\partial t}\right)^n+\mathcal{O}(\Delta t^2) \tag{17}$$

with

$$\frac{\partial H_\beta}{\partial t}=\frac{\partial H_\beta^I}{\partial t}-\frac{\partial H_\beta^v}{\partial t}$$

The time derivative of $\partial H_\beta^I/\partial t$ is written as

$$\left(\frac{\partial H_\beta^I}{\partial t}\right)^n=\left(\frac{\partial H_\beta^I}{\partial W_\ell}\frac{\partial W_\ell}{\partial t}\right)^n \tag{18}$$

since H_β^I depends on the W_ℓ only. The derivative $\partial W_\ell/\partial t$ in the above expression is approximated similarly as in Eq. (9), that is,

$$\left(\frac{\partial W_\ell}{\partial t}\right)^n=\left[2a\frac{\Delta W_\ell}{\Delta t}-(1-2a)\frac{\partial H_{\beta\ell}}{\partial x_\beta}+b\frac{\partial H_{\beta\ell}^I}{\partial W_m}\frac{\partial}{\partial x_\beta}(\Delta W_m)\right]^n \tag{19}$$

Now, the linearization in time of the viscous terms follows the procedure used in Ref. 6. The time derivative of H_β^v is developed according to

$$\left(\frac{\partial H_\beta^v}{\partial t}\right)^n=\left[\frac{\partial H_\beta^v}{\partial W_\ell}\frac{\partial W_\ell}{\partial t}+\frac{\partial H_\beta^v}{\partial q_{\ell\epsilon}}\frac{\partial}{\partial t}\left(\frac{\partial W_\ell}{\partial x_\epsilon}\right)\right]^n$$

in which H_β^v has been considered as depending on the independent variables

$$W_\ell,\quad \frac{\partial W_\ell}{\partial x_\beta}=q_{\ell\beta}$$

with $\ell=1,\ldots,5$ and $\beta=1,2,3$. The above expression is rearranged as

$$\left(\frac{\partial H_\beta^v}{\partial t}\right)^n=\left[\left(\frac{\partial H_\beta^v}{\partial W_\ell}-\frac{\partial^2 H_\beta^v}{\partial x_\epsilon \partial q_{\ell\epsilon}}\right)\frac{\partial W_\ell}{\partial t}\right]^n+\frac{\partial}{\partial x_\epsilon}\left(\frac{\partial H_\beta^v}{\partial q_{\ell\epsilon}}\frac{\partial W_\ell}{\partial t}\right)^n \tag{20}$$

and simplification in the first bracket of the right-hand side occurs if the variations of λ and μ are neglected in the above expression (see Ref. 6). As in the one-dimensional method, the derivative $(\partial W_\ell/\partial t)^n$ is approximated with the standard formula

$$\left(\frac{\partial W_\ell}{\partial t}\right)^n=\frac{W_\ell^{n+1}-W_\ell^n}{\Delta t}\equiv\frac{\Delta W_\ell^n}{\Delta t} \tag{21}$$

By taking account of Eqs. (18) to (21), the integral form of Eq. (17) is

$$\begin{aligned}&\int\int\int_v\frac{\Delta W^n}{\Delta t}dv+\int\int_s\left\{a\Delta t\frac{\partial H_\beta^I}{\partial W_\ell}\frac{\Delta W_\ell}{\Delta t}\right.\\&\left.+b\frac{\Delta t}{2}\frac{\partial H_\beta^I}{\partial W_\ell}\left[\frac{\partial H_{\epsilon\ell}^I}{\partial W_m}\frac{\partial(\Delta W_m)}{\partial x_\epsilon}\right]\right\}^n N_\beta ds\\&-\frac{1}{2}\int\int_s\Delta t\left[\left(\frac{\partial H_\beta^v}{\partial W_\ell}-\frac{\partial^2 H_\beta^v}{\partial x_\epsilon\partial q_{\ell\epsilon}}\right)\frac{\Delta W_\ell}{\Delta t}\right.\\&\left.+\frac{\partial}{\partial x_\epsilon}\left(\frac{\partial H_\beta^v}{\partial q_{\ell\epsilon}}\frac{\Delta W_\ell}{\Delta t}\right)\right]^n N_\beta ds\\&=-\int\int_s\left(H_\beta-\frac{1-2a}{2}\Delta t\frac{\partial H_\beta^I}{\partial W_\ell}\frac{\partial H_{\epsilon\ell}}{\partial x_\epsilon}\right)^n N_\beta ds\end{aligned} \tag{22}$$

As explained in the previous section, the purely explicit part of the scheme appearing in the right-hand side of Eq. (22) is replaced by

$$\int\int\int_v\left[\left(\frac{\hat{W}^{n+1}-W^n}{\Delta t}\right)\right]dv$$

where $\hat{W}^{n+1}$ is given by a predictor-corrector scheme similar to Eq. (13).

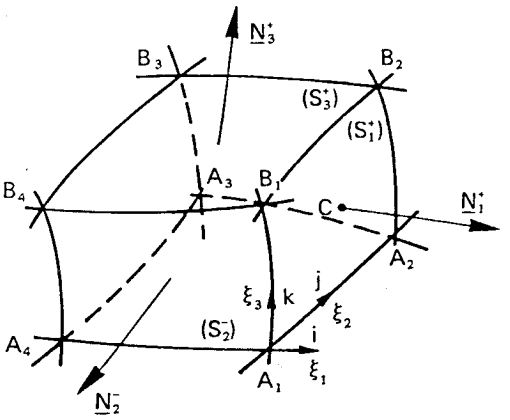

Fig. 2 The cell $\Omega(i,j,k)$.

Space Discretization

The finite volume technique previously used for the solution of the two-dimensional Euler equations[16] is applied to approximate Eq. (22). Curvilinear coordinates ξ_1, ξ_2, and ξ_3 (referenced with indices i, j, and k, respectively) are introduced to define the mesh cells into which the equations of motion are integrated. Hence, the method provides a mean value of the solution into each mesh cell and at each time step. This mean value $W_{i,j,k}^n$ is assumed to be located at the center $(x_\beta)_{i,j,k}=x_\beta(i\Delta\xi_1,\ j\Delta\xi_2,\ k\Delta\xi_3)$ of the cell $\Omega(i,j,k)$ described in Fig. 2.

The general procedure of the calculation will now be outlined.

The Explicit Step

First, as with the explicit scheme (13), the provisional value $\hat{W}_{i,j,k}^{n+1}$ is determined by

$$\left(\frac{\hat{W}^{n+1}-W^n}{\Delta t}v\right)_{i,j,k}=-\sum_{\eta=1}^{3}(F_\eta^+ + F_\eta^-) \tag{23}$$

where v is the volume of the mesh cell Ω (i,j,k), F_η^+ and F_η^- refer to the fluxes through the sides S_η^+ and S_η^-, respectively. It should be noted that the subscript $\eta=1,2,3$ refers to the mesh directions i, j, k, respectively (see Fig. 2). The fluxes are defined according to Eq. (13b) considered in the finite volume formulation. For example, the flux F_1^+ through the side S_1^+, is defined by

$$\begin{aligned}F_1^+=&\left[\frac{1-2a}{2\alpha}H_\beta^I(\tilde{f}^{n+\alpha})+\left(1-\frac{1-2a}{2\alpha}\right)H_\beta^I(\tilde{f}^n)\right.\\&\left.-H_\beta^v\left(\tilde{f}^n,\frac{\partial f^n}{\partial x},\frac{\partial f^n}{\partial x_2},\frac{\partial f^n}{\partial x_3}\right)\right]_{i+\frac{1}{2},j,k}S_{1\beta}^+\end{aligned} \tag{24}$$

where H_β^I and H_β^v are expressed in terms of the primitive variables $f=(f_\ell)=(\rho,\ u_1,\ u_2,\ u_3,\ e)$, $(\ell=1,\ldots,5)$ with

$$f^n=f(W_m^n),\quad m=1,\ldots,5,\quad \tilde{f}_{i+\frac{1}{2},j,k}^{n+\alpha}=f[(\tilde{W}_m^{n+\alpha})_{i+\frac{1}{2},j,k}]$$

$$\tilde{f}_{i+\frac{1}{2},j,k}^n=(f_{i,j,k}^n+f_{i+1,j,k}^n)/2$$

and $W^{n+\alpha}_{i+\frac{1}{2},j,k}$ a predicted mean value of the solution at time level $n+\alpha$. The surface vector $\underline{S}_1^+ = S_1^+ \underline{N}_1^+ = (S_{1\beta}^+)$ of the side S_1^+ (see Fig. 2), is evaluated from

$$\underline{S}_1^+ = \tfrac{1}{2}(\underline{A}_1 B_2 \times \underline{A}_2 B_1)$$

The expression of the volume v in Eq. (23) is given by

$$v = (1/16)[A_1B_3 \cdot (A_2B_4 \times A_3B_1) + A_2B_4 \cdot (A_3B_1 \times A_4B_2) + A_3B_1 \cdot (A_4B_2 \times A_1B_3) + A_4B_2 \cdot (A_1B_3 \times A_2B_4)]$$

The predicted mean value $\tilde{W}^{n+\alpha}_{i+\frac{1}{2},j,k}$ is defined into a shifted cell $\tilde{\Omega}(i+\frac{1}{2}, j, k)$ centered at point C of the side S_1^+ (see Figs. 2 and 3) by

$$\left(\frac{\tilde{W}^{n+\alpha}\tilde{v} - \overline{W^n_v}}{\alpha \Delta t}\right)_{i+\frac{1}{2},j,k} = -\sum_{\eta=1}^{3} (G_\eta^+ + G_\eta^-) \tag{25}$$

with, for example,

$$G_1^+ = \left[H_\beta^I(f) - \theta H_\beta^v\left(f, \frac{\partial f}{\partial x_1}, \frac{\partial f}{\partial x_2}, \frac{\partial f}{\partial x_3}\right)\right]^n_{i+1,j,k} \tilde{S}_{1\beta}^+ \tag{26a}$$

$$G_2^+ = \left[H_\beta^I(\bar{f}) - \theta H_\beta^v\left(\bar{f}, \frac{\partial f}{\partial x_1}, \frac{\partial f}{\partial x_2}, \frac{\partial f}{\partial x_3}\right)\right]^n_{i+\frac{1}{2},j+\frac{1}{2},k} \tilde{S}_{2\beta}^+ \tag{26b}$$

where

$$\bar{f}^n_{i+\frac{1}{2},j+\frac{1}{2},k} = (f^n_{i,j,k} + f^n_{i+1,j,k} + f^n_{i,j+1,k} + f^n_{i+1,j+1,k})/4$$

and similar expressions for the other fluxes.

The components $\partial f_\ell / \partial x_\beta$ of the derivatives $\partial f / \partial x_\beta$, which appear in the viscous term H_β^v, are evaluated at the center of the sides $S_\eta^\pm$ and $\tilde{S}_\eta^\pm$ by centered finite difference formulas. More precisely, let $\phi(=f_\ell$ or $W_\ell)$ be defined at the six points N, P, Q, R, S, and T, surrounding a central point M, its gradient at the point is expressed by

$$(\text{grad } \phi)_M = \left(\frac{\partial \phi}{\partial x_\beta}\right)_M = \frac{\phi_{PN}(\underline{RQ} \times \underline{ST}) + \phi_{RQ}(\underline{ST} \times \underline{PN}) + \phi_{ST}(\underline{PN} \times \underline{RQ})}{\underline{PN}(\underline{RQ} \times \underline{ST})} \tag{27}$$

with

$$\phi_{PN} = \phi_N - \phi_P \ldots.$$

Figure 4 shows the mesh point ordering when Eq. (27) is used to calculate the gradient components of f_ℓ at the side ζ (i.e., S_1^+ or $\tilde{S}_1^+$). To be more exact, let us denote by (i,j,k) the center of the cell $\Omega(i,j,k)$. Table 1 gives the mesh indices of the different points for the cases $\zeta = S_1^+$ and $\zeta \tilde{S}_1^+$. For the boundary cells, noncentered difference formulas in the direction transversal to the boundary are used in Eq. (27).

The other fluxes $F_{2,3}^\pm$ occurring in Eq. (23) are calculated in the same manner using predicted values in shifted cells in the directions j and k, respectively.

The Implicit Step

Equation (22) is considered for a cell $\Omega(i,j,k)$, and its approximation leads to

$$\left(\frac{\Delta W^n}{\Delta t} v\right)_{i,j,k} + \sum_{\eta=1}^{3} (E_\eta^+ + E_\eta^-) = \left(\frac{\hat{W}^{n+1} - W^n}{\Delta t} v\right)_{i,j,k} \tag{28}$$

where E_η^+ and E_η^- are the fluxes through the sides S_η^+ and S_η^-, respectively. Each of the flux terms is split into two parts according to the presence or absence of the space derivatives of ΔW^n. For example,

$$E_1^+ = A_1^+ - B_1^+ \tag{29}$$

The term A_1^+, which does not contain space derivatives of ΔW^n, is written as

$$A_1^+ = \Delta t\left[a \frac{\partial H_\beta^I}{\partial W_\ell}(\bar{f}) - \frac{1}{2}\frac{\partial H_\beta^v}{\partial W_\ell}\left(\bar{f}, \frac{\partial f}{\partial x_1}, \frac{\partial f}{\partial x_2}, \frac{\partial f}{\partial x_3}\right) + \frac{1}{2}\frac{\partial^2 H_\beta^v}{\partial x_\epsilon \partial q_{\ell\epsilon}}\left(\bar{f}, \frac{\partial f}{\partial x_1}, \frac{\partial f}{\partial x_2}, \frac{\partial f}{\partial x_3}\right)\right]^n_{i+\frac{1}{2},j,k} \times \left(\frac{\overline{\Delta W}_\ell}{\Delta t}\right)^n_{i+\frac{1}{2},j,k} S_{1\beta}^+ \tag{30}$$

where the components $\partial f_\ell / \partial x_\beta$ of $\partial f / \partial x_\beta$ are evaluated with Eq. (27).

The term B_1^+, which contains space derivatives of ΔW^n, is much more complicated than A_1^+. In order to simplify the description, only a typical part of B_1^+ is considered, namely,

$$\frac{\Delta t}{2}\left\{\frac{\partial}{\partial x_1}\left[\frac{\partial H_\beta^v}{\partial q \ell_1}(f)\frac{\Delta W_\ell}{\Delta t}\right]^n\right\}_{i+\frac{1}{2},j,k} S_{1\beta}^+$$

The x_1 derivative is approximated by means of Eq. (27). Consequently, the values of ΔW^n in the six adjacent cells will appear in the approximate. The contributions in the j and k directions would make difficult a subsequent splitting of the three-dimensional operator into a sequence of one-dimensional operators. Therefore, the contributions in these directions have been ignored, the resulting error disappearing at steady state. In this way, in the approximation of Eq. (29), only values of ΔW^n at (i,j,k) and $(i+1, j, k)$ occur.

Thus, Eq. (28) can be put into the form

$$(1 + \Lambda_1 + \Lambda_2 + \Lambda_3)^n \Delta W^n_{i,j,k} = (\hat{W}^{n+1} - W^n)_{i,j,k} \tag{31}$$

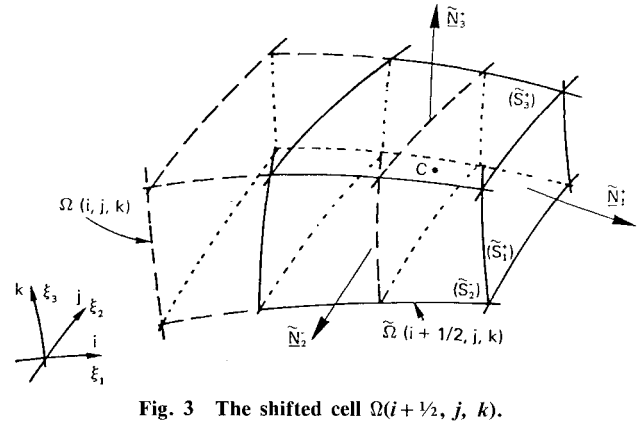

Fig. 3 The shifted cell $\Omega(i+\frac{1}{2}, j, k)$.

Table 1 Mesh indices of points occurring in Fig. 4 for S_1^+ and $\tilde{S}_1^+$

	ζ	
	S_1^+	$\tilde{S}_1^+$
M	$i+\frac{1}{2}, j, k$	$i+1, j, k$
N	$i+1, j, k$	$i+2, j, k$
P	i, j, k	i, j, k
Q	$i+\frac{1}{2}, j+1, k$	$i+1, j+1, k$
R	$i+\frac{1}{2}, j-1, k$	$i+1, j-1, k$
S	$i+\frac{1}{2}, j, k+1$	$i+1, j, k+1$
T	$i+\frac{1}{2}, j, k-1$	$i+1, j, k-1$

where Λ_1, Λ_2, and Λ_3 are three-point finite difference operators in the directions i, j, and k, respectively.

The solution $\Delta W^n_{i,j,k}$ of Eq. (31) is calculated from the Douglas-Gunn splitting procedure (see Ref. 4, e.g.),

$$(1+\Lambda_2)^n \Delta W^*_{i,j,k} = (\hat{W}^{n+1} - W^n)_{i,j,k} \tag{32a}$$

$$(1+\Lambda_3)^n \Delta W^{**}_{i,j,k} = \Delta W^*_{i,j,k} \tag{32b}$$

$$(1+\Lambda_1)^n \Delta W^{***}_{i,j,k} = \Delta W^{**}_{i,j,k} \tag{32c}$$

$$W^{n+1}_{i,j,k} = W^n_{i,j,k} + \Delta W^{***}_{i,j,k} \tag{32d}$$

Therefore, at each time step, only block-tridiagonal matrices must be inverted. At steady state, the solution is given by

$$(\hat{W}^{n+1} - W^n)_{i,j,k} = 0$$

that is to say, by the explicit part of the scheme.

IV. Numerical Applications

The method has been implemented on a CDC-CYBER 750 in order to compute transonic flows at moderate Reynolds number over a swept wing at zero angle of attack.

In the first application, the wing is bounded by two planes that are parallel to the freestream direction, and conditions of symmetry are prescribed at these planes. This first configuration was chosen in order to avoid the treatment of the wing tip.

The second application deals with the flow around the finite wing ONERA M6. For both applications, the Reynolds number based on the chord of the profile is $Re_\infty = 1000$ and the Mach number is $M_\infty = 0.8$. The wing section is a NACA0012 profile for the first application, with the ONERA-D profile for the second one.

Computational Domain and Boundary Conditions

Due to the symmetry of the flow, the computational domain is restricted to the upper half of the flow (see Fig. 5). The limitation in the central core memory of the CYBER-750 has required us to develop the calculations plane by plane in the i direction. This procedure leads to the ordering of the implicit one-dimensional steps in Eq. (32).

The inflow and outflow boundaries pass through the center of the cells. All of the other boundaries, including the wing, follow the sides of the cells.

The conditions of symmetry are easy to prescribe. Here we shall describe only the treatment of the conditions on the wing and at the inflow and outflow boundaries.

On the wing, which is the side S_3^- of the cell Ω $(i,j,1)$, the fluxes are evaluated taking account of the no-slip and adiabatic conditions. Moreover, this evaluation requires knowledge of the pressure on the wing. At the explicit step, this pressure is calculated from a noncentered differencing of the normal momentum equation. At the implicit step, the pressure at the wall, needed for the solution of Eq. (32b), is evaluated from the condition $\partial p/\partial \xi_3 = 0$. Therefore, the implicit flux on the wing is calculated with the conditions

$$\Delta \underline{U}^{**} = \underline{0}, \quad \frac{\partial \Delta e^{**}}{\partial \xi_3} = 0, \quad \frac{\partial \Delta p^{**}}{\partial \xi_3} = 0$$

where the ξ_3-derivative is approximated with a first-order formula.

The flow in the region close to the inflow boundary is assumed to be inviscid, and the viscous terms are neglected in the governing equations. Since the normal velocity is subsonic at the inflow boundary, only four boundary conditions need be prescribed. In the present calculations, the values of entropy, total enthalpy, and flow direction are prescribed. The supplementary condition is provided by the compatibility relation[17] associated with the outgoing characteristic

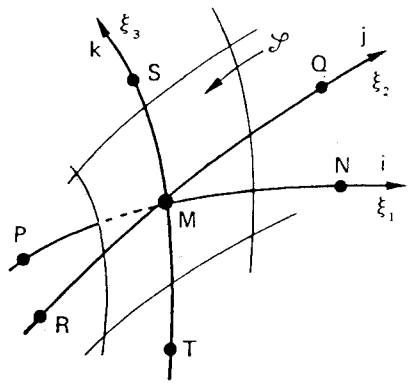

Fig. 4 Typical mesh points used in Eq. (27) at the side $\zeta(S_1^+ + \tilde{S}_1^+)$.

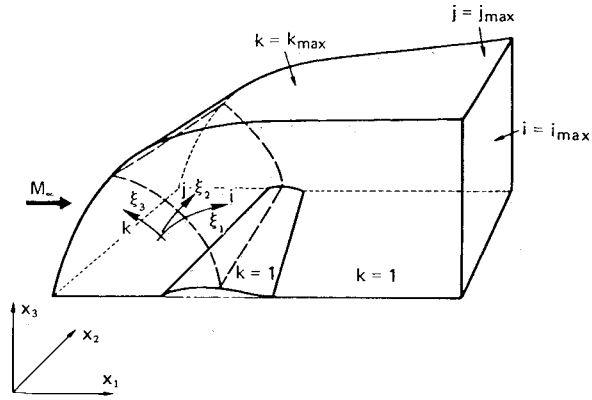

Fig. 5 Typical computational domain.

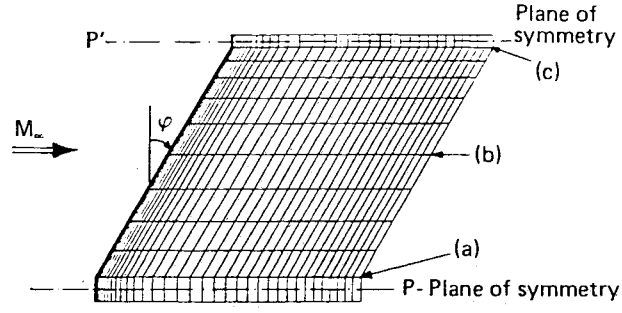

Fig. 6 Mesh on the wing and definition of sections a, b, and c.

$$p^{n+1} - p_s^{n+1} + (\rho c)^n (\underline{U}^{n+1} - \underline{U}_s^{n+1})\underline{N} = 0$$

where $c^2 = \gamma_p/\rho$, $\underline{N}$ is the outward unit vector normal to the boundary. The subscript s refers to the values at the inflow boundary obtained by extrapolation from the solution at the inner cells. The above conditions are used after the implicit step, the variations of the solution at the boundary being ignored during this implicit step.

In the outflow boundary cells, the unknowns are extrapolated from the inner cells for the calculation of the implicit i step, which provides the final values of velocity and temperature. Then, the final pressure is set equal to its freestream value and the final density is calculated from the state equation.

Results

The calculations presented here were made with a spatially varying time step deduced from the approximate explicit

criterion

$$\Delta t_{i,j,k} = \eta \min(\Delta t_1, \Delta t_2) \qquad (\eta = ct > 0)$$

$$\Delta t_1 = [d/(|\underline{U}| + c)]_{i,j,k}$$

$$\Delta t_2 = (\rho Pr Re_\infty / 2\gamma\mu g)_{i,j,k} \tag{33}$$

where d is the shortest distance between the center of the mesh cell $\Omega(i,j,k)$ and the center of the six adjacent cells in the mesh directions i, j, and k. The expression of g in Eq. (33) is given by

$$g = (\text{grad}\xi_\beta / \Delta\xi_\beta)^2$$

where the gradient components of the curvilinar coordinates ξ_β ($\beta = 1,2,3$) are evaluated with Eq. (27) involving the six above-mentioned cells.

In the present results, the relation (12) between the parameters b and a was used, and a different value of a (denoted a_1, a_2, and a_3) was chosen in each direction of the mesh. For our purpose, $\alpha = \frac{1}{2}$, and no artificial viscosity was added.

For the calculations of the flow around a wing between two parallel planes, the mesh is shown in Figs. 6 and 7. It involves $51 \times 21 \times 12$ cells in the directions i, k, and j, respectively.

Two-Dimensional Airfoil

First of all, the three-dimensional code has been applied when the sweep angle is $\varphi = 0$ deg, corresponding to a two-dimensional flow in the direction (x_1, x_3); that is to say, there is no change of the solution in the j direction that corresponds to ξ_2 and also to x_2. With $a_1 = a_3 = \frac{1}{2}$, the method did not converge. Good numerical results have been obtained for $a_1 = a_3 = 0$, and $\theta = 1$. However, similar results have been achieved more rapidly for $a_1 = a_3 = 0.4$ and $\theta = 1$. In this case, the local time step was calculated from Eq. (33) with $\eta = 9.75$. Preliminary explicit calculations indicate that this value of η is 13 times greater than the maximal value ($\eta = 0.75$), ensuring stability. In these calculations, the explicit scheme used corresponds to the explicit step alone [Eqs. (23-26)] with $\alpha = 1 + \sqrt{5}/2$, $\theta = 1$, and $a_1 = a_2 = a_3 = 0$; artificial viscosity is added.

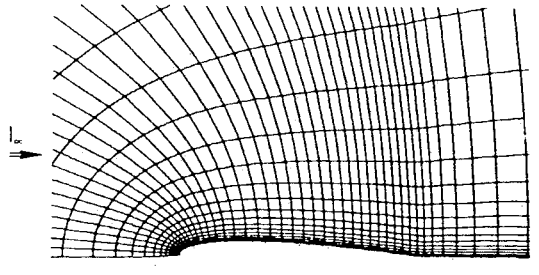

Fig. 7 Mesh in section a, b, or c (51×21 cells).

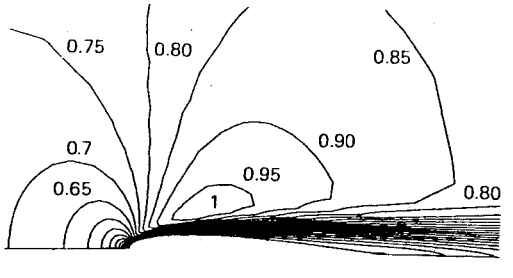

Fig. 8 Iso-Mach lines for $\varphi = 0$ deg.

Results of the implicit calculations are displayed in Figs. 8 and 9. The iso-Mach lines are shown in Fig. 8. The convergence history is plotted in Fig. 9 through the residues R_1, the total drag coefficient CD, and the pressure drag coefficient CDP. Figure 9 also shows the residues obtained after 1500 iterations of the explicit scheme (about 4500 iterations are needed to obtain residues of the order of 10^{-4}).

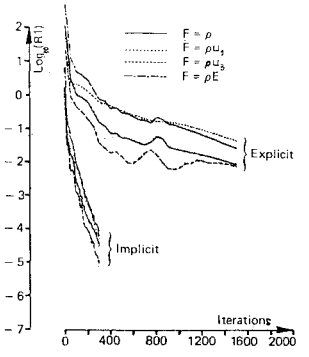

a) Maximal residues $R_1 = \max_{i,k} |F^{n+1}_{i,k} - F^n_{i,k}/\Delta t_{i,k}|$ comparison between implicit and explicit calculations.

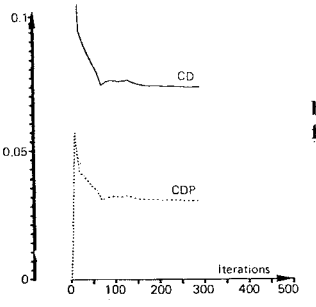

b) Drag coefficients CD and CDP for the implicit calculation.

Fig. 9 Convergence history for $\varphi = 0$ deg.

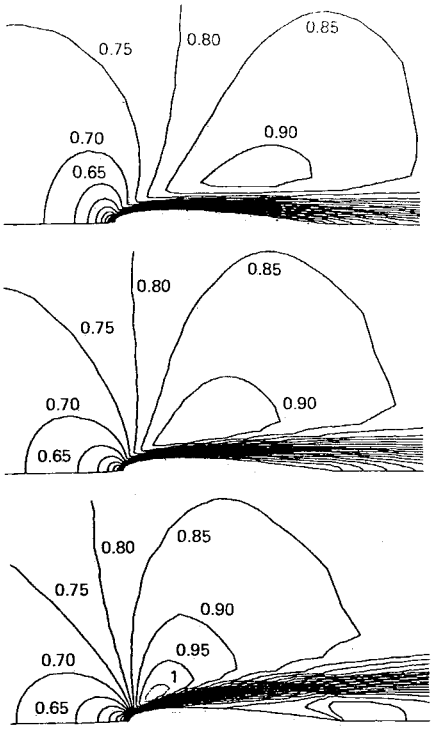

Fig. 10 Iso-Mach lines for $\varphi = 30$ deg in sections a, b, and c defined in Fig. 6.

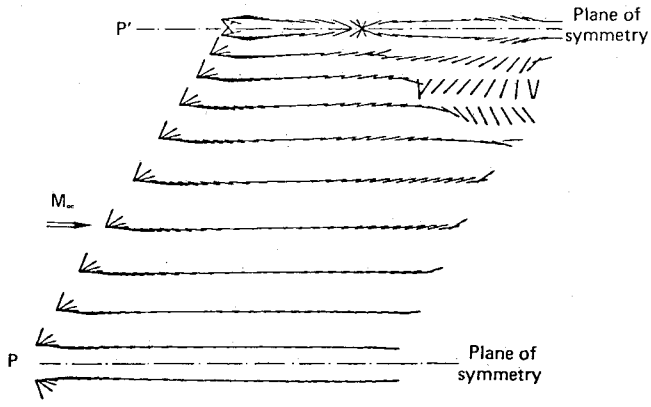

Fig. 11 Direction of the skin friction on the wing for $\varphi = 30$ deg.

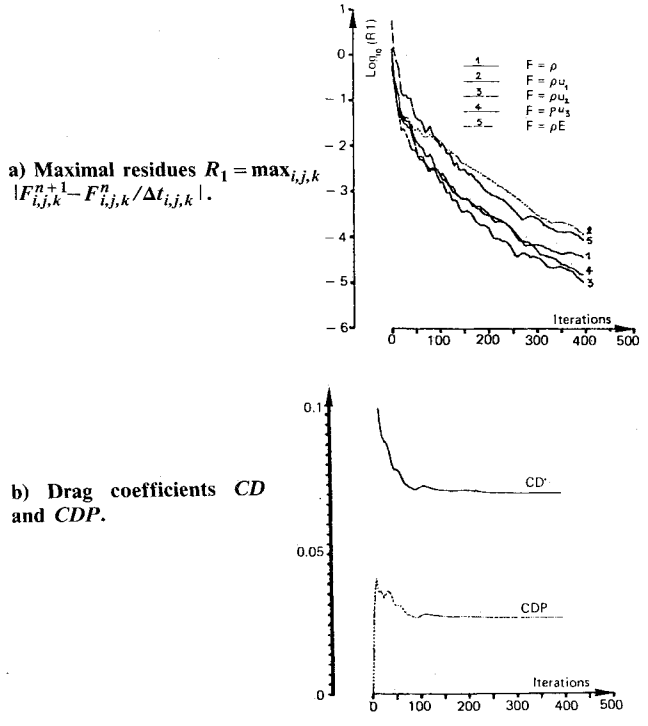

Fig. 12 Convergence history for $\varphi = 30$ deg.

Wing Between Two Parallel Planes

In the case $\varphi = 30$ deg, the three-dimensional results are described in Figs. 10-12. The numerical solution predicts a reverse flow region near the trailing edge of the wing in the vicinity of the plane of symmetry P' (see also Fig. 6). This solution has been obtained after 400 iterations with a local time step deduced from Eq. (33) with $\eta = 7.5$ and for $a_1 = a_3 = 0.4$, $a_2 = 0$, and $\theta = 1$. the iso-Mach lines in various sections of the wing are shown in Fig. 10. It should be noted that in Fig. 10c there is a supersonic zone in the flowfield and a large reverse flow region. Figure 11 shows the reverse flow region through a plotting of the direction of the skin friction on the wing. Finally, Fig. 12 gives the convergence history. The present solution requires 27,000 s of CPU time on a CDC-CYBER 750 (67.5 s/time step or 5.25 10^{-3} s/cell/time step). An explicit calculation of this configuration would involve large computing costs. Therefore, it has not been possible to perform such a calculation with a sufficient degree of convergence, allowing a significant comparison with the implicit method.

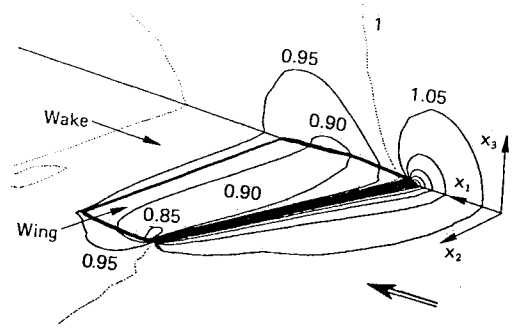

Fig. 13 Isobar lines (p/p_∞) on the wing, in the plane of the wing, and in the first section in the vicinity of the wing root.

Finite Wing ONERA M6

The C-O type mesh used for the finite wing involves $51 \times 17 \times 21$ cells in the directions i, k, and j, respectively. The solution presented in Fig. 13 through the isobar lines on the wing, in the plane of the wing and in the plane of symmetry, was reached after 560 time steps of the scheme $a_1 = a_2 = a_3 = 0$ and $\theta = 0$. These results correspond to residues R_1 lower than 10^{-3}. The local time step is deduced from Eq. (33) with $\eta = 3.75$. The CPU time is about 186 s/time step (10^{-2} s/cell/time step).

V. Conclusion

A new implicit method has been developed for the solution of the compressible Navier-Stokes equations. This method retains the advantages of the Beam and Warming approach but is based on an improved Euler solver. Thus, in the inviscid limit, the present method is unconditionally stable in three dimensions, dissipative in the sense of Kreiss, and it leads to the solution of well-conditioned linear systems. The present method has been applied to the calculation of three-dimensional laminar flowfields over wings. Substantial reductions in computing time have been achieved due to the fast convergence of the implicit method. Further improvements can be looked for after a more thorough analysis has been carried out on the effect of the various parameters (α, θ, and a_1, a_2, a_3) and of the time step on the efficiency and the accuracy of the scheme.

Acknowledgments

The work described in this paper was supported in part by the "Service Technique des Programmes Aéronautiques" (STPA, French Ministry of Defense). The authors wish to thank C. Koeck for providing the mesh of wing ONERA M6.

References

[1]Peyret, R. and Viviand, H., "Computation of Viscous Compressible Flows Based on the Navier-Stokes Equations," AGARDograph-AG-212, 1975.

[2]MacCormack, R. W. and Lomax, H., "Numerical Solution of Compressible Viscous Flows," *Annual Review of Fluid Mechanics*, Vol. 11, 1979, pp. 289-316.

[3]Hollanders, H. and Viviand, H., "The Numerical Treatment of Compressible High Reynolds Number Flows," von Kármán Insitute for Fluid Dynamics, Lecture Series 1979-6, 1979.

[4]Peyret, R. and Taylor, T. D., *Computational Methods for Fluid Flow*, Springer-Verlag, New York, 1983.

[5]Briley, W. R. and MacDonald, H., "Solution of the Three-Dimensional Compressible Navier-Stokes Equations by an Implicit Technique," *Lecture Notes in Physics*, Vol. 35, 1975, pp. 105-110.

[6]Beam, R. M. and Warming, R. F., "An Implicit Factored Scheme for the Compressible Navier-Stokes Equations," *AIAA Journal*, Vol. 16, April 1978, pp. 393-402.

[7]Steger, J. L., "Implicit Finite-Difference Simulation of Flow about Arbitrary Two-Dimensional Geometries," *AIAA Journal*, Vol. 16, July 1978, pp. 679-686.

[8]MacCormack, R. W., "A Numerical Method for Solving the Equations of Compressible Viscous Flows," *AIAA Journal*, Vol. 20, Sept. 1982, pp. 1275-1281.

[9]Kordulla, W. and MacCormack, R. W., "Transonic Flow Computation Using an Explicit-Implicit Method," *Lecture Notes in Physics*, Vol. 170, Springer-Verlag, New York, 1982, pp. 286-295.

[10]Lerat, A., "Une classe de schémas implicites pour les systemes hyperboliques de lois de conservation," *Comptes-Rendus de Academie des Sciences, Paris*, No. 288A, 1979, pp. 1033-1036.

[11]Lerat, A., "Implicit Methods of Second-Order Accuracy for the Euler Equations," AIAA Paper 83-1925, 1983.

[12]Lerat, A., Sides, J., and Daru, V., "Efficient Computation of Steady and Unsteady Transonic Flows by an Implicit Solver," in *Advances in Computational Transonics*, edited by W. G. Habashi, Pineridge Press, Swansea, U.K., 1984.

[13]Beam, R. M. and Warming, R. F., "An Implicit Finite-Difference Algorithm for Hyperbolic Systems in Conservation-Law Form," *Journal of Computational Physics*, Vol. 22, Sept. 1976, pp. 87-110.

[14]Thommen, H. U., "Numerical Integration of the Navier-Stokes Equations," *Zeitschrift für angewandte Mathematik und Physik*, No. 17, 1966, pp. 369-384.

[15]Lerat, A., "Implicit Time-Dependent Methods for the Solution of the Euler Equations I—Analysis of the Methods," von Kármán Institute for Fluid Dynamics, Lecture Series 1984-04, 1984.

[16]Lerat, A. and Sides, J., "A New Finite-Volume Method for the Euler Equations with Applications to Transonic Flows," in *Numerical Methods in Aeronautical Fluid Dynamic*, edited by P. L. Roe, Academic Press, New York, 1982, pp. 245-288.

[17]Viviand, H. and Veuillot, J. P., "Pseudo-Unsteady Methods for Transonic Flow Calculations," ONERA Publication No. 1978-4, 1978 (English version, ESA-TT-549, Feb. 1979).